Brightness-dependent Tarpley model for global solar radiation estimation using GOES satellite images: application to Uruguay

R. Alonso Suárez[a], G. Abal[a], R. Siri[a], P. Musé[b]

[a]*Instituto de Física, Facultad de Ingeniería*
[b]*Instituto de Ingeniería Eléctrica, Facultad de Ingeniería*
Universidad de la República, Herrera y Reissig 565, CP 11300, Montevideo, Uruguay

Abstract

A statistical model based on Tarpley's original solar irradiation model is proposed and evaluated using data from seven new ground stations in Uruguay. The model estimates hourly global solar irradiation on a horizontal surface using GOES-East satellite images. We show that the introduction of a simple brightness dependence in the model parameters drastically improves the accuracy of the estimates. The implementations of the original and the improved models are explained in detail. For each case, the parameters are adjusted using controlled quality solar irradiation data and a comprehensive performance analysis, on an hourly and daily basis, is carried out using data from independent measurement sites. The relative RMS deviations for the estimates of the brightness-dependent model are 7.1% for the daily estimates and 14.0% for the hourly estimates, relative to the mean of the measurements. This represents a reduction of approximately 45% (daily) and 25% (hourly) in the relative RMS deviations of the original model. The improved model provides a good balance between simplicity and accuracy.

Keywords: solar irradiation, statistical model, remote sensing, GOES satellite images.

1. Introduction

Reliable solar resource estimates are essential to design systems for conversion of solar energy into useful (thermal, electrical) energy. Information on an hourly basis is needed to estimate the output of solar energy conversion devices or to properly assess their performance. Knowledge about the solar resource spatial and temporal distribution is also important for agricultural planning and research. At most locations in Uruguay, reliable solar irradiation ground data are not available as this variable is not currently included among the routine meteorological measurements done by the meteorological service.

Schemes based on ground measurements and interpolation techniques provide limited accuracy, even over relatively small distances, due to highly variable atmospheric conditions. Simple satellite-based models can provide better accuracy for hourly irradiation than ground measurement interpolation. In fact, from an end–user perspective, it is preferable to rely on satellite-based hourly estimates than using ground data from stations located more than 30 km away of the target point (Perez et al., 1997).

Satellite-based solar resource models used to be classified in two categories: statistical and physical (Noia et al., 1993a,b). Physical models attempt to describe the radiative transfer process in the earth–atmosphere system and rely on information about the current composition and state of the atmosphere, which may not be available for all locations. However, these models can be used to estimate solar irradiation in regions where no ground radiation measurements are available. On the other hand, statistical models rely on regression techniques between satellite information and simultaneous ground measurements for the same location in order to adjust their parameters. Most modern models are of a hybrid nature, i.e. they have a physical basis and include some adjustable parameters. Among the most popular satellite-based radiation models are the SUNY model (Perez, 2002) and the Heliosat family models. In particular, the Heliosat 2 model (Hammer, 2003, Rigollier, 2004) is widely documented. Both models take advantage of highly tuned clear sky models and cloud cover is considered by the use of a cloud index derived from satellite images. Region-specific modifications of Heliosat 2 empirical relationship between the cloud index and the clear sky index have been proposed in (Zarzalejo et al., 2009), reaching better results in terms of irradiation estimates performance. For recent reviews on satellite-based solar radiation models see (Stoffel et al., 2010, Chap. 4), or (Polo et al., 2008).

Tarpley's original model is one of the earliest satellite-based statistical irradiation models. In the original proposal (Tarpley, 1979), applied to the Great Plains area in the U.S., the ratio of cloudy vs. clear-sky squared brightness counts was used to introduce cloudiness information in the model and this resulted in a significant bias error. A second version, based on the difference of the squared brightness counts, significantly reduced the bias problem (Justus et al., 1986). In this work, we refer to this last model as the JPT model (for Justus, Paris, Tarpley). In spite of its simplicity and reasonable performance in snow-free areas, this model seems to have been forgotten and is now considered somewhat outdated. In spite of this, local implementations and evaluations of the JPT model for the South American plains have been recently reported. In (Righini and

Barrera, 2008) daily solar irradiation was estimated for part of Argentina and a relative RMS of 17.3% against ground data was reported. In Alonso et al. (2011), preliminary results for the first implementation of Tarpley's model in Uruguay show a relative RMS of 12% against independent ground data, also on a daily basis. In this work, we briefly review this last implementation and propose a new version of the JPT model which significantly improves the accuracy of the estimates while preserving the simple character of the original model. We show that this improved model, which we call BD-JPT due its brightness dependence, can provide a very good agreement with independent ground measurements when its parameters are locally derived. This model may be used on a regional scale, including the whole of Uruguay, the eastern part of Argentina and the southeren states of Brasil.

This article is organized as follows. Section 2 describes the JPT model in detail and existing performance reports are discussed. The solar irradiation ground data and satellite images used in this work are described in Section 3. In Section 4, the local implementation of this model to the target area considered in this work is summarized and in Section 5, an improved version of the model is derived, explained and evaluated. Performance indicators for both models are discussed in Section 5.3. Finally, our conclusions are presented in Section 6.

2. The JPT model

Following Justus et al. (1986), in the standard JPT model hourly global irradiation on a horizontal plane at ground level, I, is parameterized as

$$I = I_{sc}\left(\frac{r_0}{r}\right)^2 \cos\theta_z \left(a + b\cos\theta_z + c\cos^2\theta_z\right) + d\left(B_m^2 - B_0^2\right) \quad (1)$$

where I is expressed in kJ/m^2 and $I_{sc} = 4921$ kJ/m^2 is the hourly integral of the Solar Constant. The factor $(r_0/r)^2$ accounts for the variation of the Sun-Earth distance r (assumed constant within a day) with respect to its mean value r_0 and it depends on the day number n. The solar zenith angle, θ_z, is the angle formed by the Sun-observer direction with the local vertical. It depends on location, day number and local time in the usual way (Iqbal, 1983). The hourly averages of $\cos\theta_z$ and its powers are used in Eq. (1). In this expression, terms with coefficients a, b and c represent the clear-sky part of the model, while the last term introduces the cloudiness information obtained directly from the satellite counts in the visible channel and d is a conversion factor from squared brightness counts to physical irradiation units. B_m is the hourly mean brightness in a small cell which represents the neighbourhood of a given location, and B_0 is the mean clear-sky brightness for the same time and location. The presence of clouds increases the reflection towards the satellite radiometer so $B_m \geq B_0$ and the coefficient d in Eq. (1) must be negative. We have normalized the brightness counts with a factor of 2^8, chosen so that d is of order 1 which leads to a better conditioned regression problem.

2.1. Mean Brightness determination

The values of B_m and B_0 must be computed for every hourly interval and site. Effects due to cloud dynamics within the hour and instability in the satellite sensor are reduced by averaging the brightness counts over a small spatial neighbourhood of a given position. We use cells of 10 min × 10 min latitude-longitude intervals centered at the latitude and longitude (ϕ, ψ) of the location of interest. These cells represent a ground area of about 16 km × 19 km. For each cell, the mean brightness B_m is calculated as the simple average of all pixels in the cell using all the available images within the hour (i.e., images in the time interval 10:30 to 11:29 are assigned the to hour label 11). The time label in the data are in local Standard Time (UTC-3). In this way, a mean brightness $B_m(\phi, \psi)$ is obtained for each daytime hour and location. In Fig. 1 we show the distribution of the B_m values obtained from the images for three particular locations. The B_m for other locations are similarly distributed.

We shall now address the estimation of the clear-sky brightness, B_0. Following Tarpley (1979), the time dependence of the B_0 values for a cell at (ϕ, ψ) can be parameterized as

$$\begin{aligned} B_0(\phi,\psi) \;=\; & A(\phi,\psi) + B(\phi,\psi)\cos\theta_z + \\ & C(\phi,\psi)\sin\theta_z\cos\gamma + \\ & D(\phi,\psi)\sin\theta_z\cos^2\gamma \end{aligned} \quad (2)$$

where γ is the azimuth angle between the Sun and satellite directions for the location of interest. The first two terms in Eq. (2) account for the changing incident flux with local time, day and location plus a constant offset value. The other two terms are intended to account for changes in target brightness due to surface shadows and anisotropic scattering. Once the $\{A, B, C, D\}$ parameters are determined for each site, Eq. (2) is used to obtain the characteristic clear-sky brightness for a given time and location. Note that these parameters are site-specific and do not depend on the hourly atmospheric conditions, but only on the long-term average.

The coefficients in Eq. (2) should be adjusted using images for clear-sky hours only. We follow the heuristic iterative procedure originally proposed in Tarpley (1979), which filters out data for hours contaminated with clouds or with insufficient scene illumination. We start by filtering out cells with corrupted B_m values or with $\cos\theta_z < 0.1$. This eliminates early morning or late afternoon hours with high air masses for which long shadows are likely to occur. Our implementation of Tarpley's proposal is described in the following pseudocode.

For each location (ϕ_i, ψ_i):
init $B^* = 2500/2^8 \approx 9.8,\ c_0 = 1.2,\ \sigma = std(\{B_m(\phi_i,\psi_i)\})$
init $B_m^0 \leftarrow \{B_m : |B_m - B^*| \leq \sigma/2\}$
init $(A^0, B^0, C^0, D^0) \leftarrow \arg\min\left\{\|B_m^0 - B_0(\phi_i,\psi_i)\|^2\right\}$
init $k = 0$
repeat
  $\{\epsilon_k\} \leftarrow \left|B_m^k - B_0(\phi_i,\psi_i,A^k,B^k,C^k,D^k)\right|$
  $\sigma^k = std(\{\epsilon_k\}),\ c_k = c_0 + 0.1\times k$
  $k = k+1,\ \{B_m^k\} \leftarrow \{B_m^{k-1} : |\epsilon_k| \leq c_k\sigma_k\}$
  $\{A^k, B^k, C^k, D^k\} \leftarrow \arg\min\left\{\|B_m^k - B_0(\phi_i,\psi_i)\|^2\right\}$

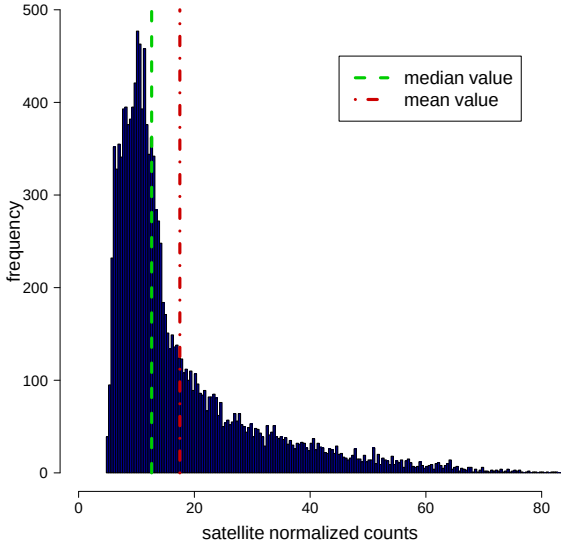

Figure 1: Histogram for mean brightness (normalized counts) for the sites coded LB, SA, TT (see Table 1). The vertical lines indicate the median (dash) and average (dash-dot) B_m values.

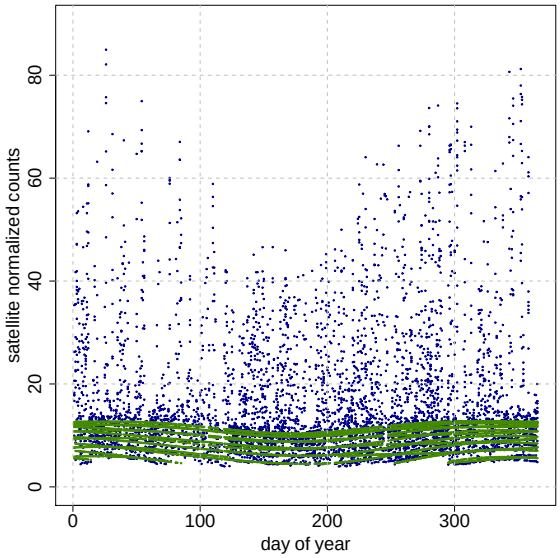

Figure 2: Values of clear-sky brightness, B_0, vs. day number, for several daytime hours, obtained from Eq. (2) (green curves). The normalized brightness counts B_m for each day are shown as blue dots. Satellite data is for the RB station, for the whole period indicated in Table 1.

until $\{B_m^k\} = \{B_m^{k-1}\}$
return $\{A, B, C, D\} \leftarrow \{A^k, B^k, C^k, D^k\}$

With these choices for B^*, c_0 and c_k, the above procedure terminates after a few iterations. Notice that the bound on the absolute residuals ϵ_k is being reduced after each iteration. This algorithm requires a first guess B^* for training and this value might be location dependent. We have chosen the initial value $B^* = 9.8$ normalized counts after visual inspection of several histograms of B_m sets, such as the one shown in Fig. 1, for different locations. We have tested the procedure with other values for B^* and found that it is not critical for the determination of the regression values. Furthermore, when the same initial value $B^* = 9.8$ is used for all the cells of our target region, visual inspection shows that reasonable values for B_0 are obtained for all of them. The result of Tarpley's algorithm for determination of B_0 is shown in Fig. 2, where the normalized mean brightness data for one site (RB, see Table 1) is compared with the clear-sky brightness B_0 (green curves) obtained from Eq. (2) for different hours in each day. Notice the weak seasonal dependence in the B_0 values, which are lower in winter than in summer.

Adjusting the parameters defined in Eq. (2) to the B_m hourly data is basically a problem of model-fitting in the presence of a large number of outliers (i.e., cloud-contaminated B_m data). We have validated the above procedure by implementing an alternative one, based on the well-known Random Sampling Consensus algorithm (RANSAC hereafter) proposed by Fischler and Bolles (1981). The RANSAC algorithm is suited to solve this kind of problems, but it requires considerably more computational effort than Tarpley's proposal. RANSAC is also an iterative procedure; in each iteration, a set of random samples from the B_m set is selected. The number of selected samples is large enough to fit a new model. Then, the residuals of the whole B_m set under this model are computed. Those with large residuals are discarded, and the model is refined by readjusting Eq. (2) with the resulting set. Finally, the total root mean square (RMS) deviation is computed and if the current model yields a smaller RMS deviation than the previously selected best model, the current model is accepted as best model. Repetition of this procedure yields an optimal solution when the number of outliers is less than half of the total number of samples. The results obtained from the RANSAC algorithm, in terms of both the final model performance and the resulting B_0 values, are similar to those obtained by our implementation of Tarpley's procedure. Since the heuristic procedure described in Tarpley (1979) is simpler and requires significantly less computational effort (usually about ten iterations) we use it to obtain the B_0 values and consider it validated by our RANSAC implementation.

2.2. Related work

In Justus et al. (1986) a set of 7200 coincident satellite and pyranometer hourly observations for the period August–December 1980 over the U.S. Great Plains was used to determine the coefficients in Eq. (1) from multiple regression. They used the adjusted model to generate irradiation estimates for the continental United States, Mexico and the central part of South America, with $1^\circ \times 1^\circ$ resolution. A common performance indicator is the Root Mean Square deviation (RMS), often expressed as a percentaje of the mean of the measurements (rRMS). On the comparison with hourly surface data Justus et al. (1986) report an rRMS of 16.2% of the observed mean. On a daily basis, against a set of 1021 site-days, they report an rRMS of 10.8%. Furthermore, this work quotes a compar-

ison of the same estimates against daily data from four sites in Argentina with an rRMS of 13.6% or 12.8% for the single site at Pergamino, equipped with a thermopile pyranometer (Espoz and Brizuela, 1983). Frulla and collaborators also compared daily estimates from the original JPT model, using the coefficients adjusted in Justus et al. (1986), with measurements for several locations in Argentina (Frulla et al., 1988) and southern Brazil (Frulla et al., 1990). In Argentina, the JTP estimates compared to 5322 daily measurements from 13 stations for the 1982-1983 period produced an rRMS of 19.6%. In Brazil, a similar study compared the same daily JTP estimates to 4404 site-days from 9 stations for the 1982-1983 period and resulted in an rRMS of 20.3%. More recently, Righini and Barrera (2008) report a local implementation of the JPT model in which the coefficients in Eq. (1) were derived from local data. This implementation used images from the GOES-8 satellite and data from 5 pyranometric stations in Argentina. The comparison between daily irradiation estimates and ground measurements for 715 site-days resulted in an rRMS deviation of 17.3%. These results suggest that the coefficients in Eq. (1) are location-dependent. Even for regions with similar climate and geographical characteristics, a local determination of the coefficients substantially improves the model accuracy. The local JPT implementation described below, has a daily rRMS of 12.8% against data from four independent stations. In fact, to the best of our knowledge, the best performance reported for the JPT model (in terms of rRMS values) is 10.8%, as reported by the authors in their original proposal by comparison against U.S. daily data (Justus et al., 1986). A table summarizing these results can be found in Alonso et al. (2011).

3. Data used for this work

In order to adjust and evaluate the irradiation models that will be presented in Sections 4 and 5, sets of simultaneous satellite and ground irradiation measurements are required. In this section we describe the data used in this work.

3.1. GOES satellite images

GOES satellite images from the visible channel are used to provide cloud cover information with a spatial resolution of about 2 km over the target territory. Hourly and daily solar irradiation estimates are generated with the same spatial resolution and compared with independent data from four ground stations distributed over the target territory. We used images from the visible channel of the GOES-East geostationary satellite operated by NOAA/NASA and located at longitude 75 ° W. The files contain images from five spectral bands (one visible, four infrared) and are available from the web site of NOAA. A local data bank was built, composed of images starting from the year 2000, acquired at a frequency of approximately two images per hour. Each image consists of an array of geo-referenced dimensionless brightness counts. Since the actual physical device operating as GOES-East has changed over time, the twelve-year image data bank is composed of images from several (GOES 8, GOES 12 and GOES 13) different radiometers. The results

site	code	device	lat.	lon.	time period used
Las Brujas	LB	K&Z	-34.67	-56.34	05/2010 :: 11/2011
Salto	SA	K&Z	-31.27	-57.89	06/2010 :: 10/2011
Treinta y Tres	TT	K&Z	-33.28	-54.17	05/2010 :: 11/2011
Buena Unión	BU	Li-Cor	-31.06	-55.60	05/2010 :: 12/2011
Piedras de Afilar	PA	Li-Cor	-34.68	-55.58	05/2010 :: 10/2011
José Ignacio	JI	Li-Cor	-34.85	-54.74	05/2010 :: 10/2011
Rincón del Bonete	RB	Li-Cor	-32.80	-56.42	05/2010 :: 10/2011

Table 1: Details of the measurement stations used in the present work. The *latitude* and *longitude* are in decimal degrees.

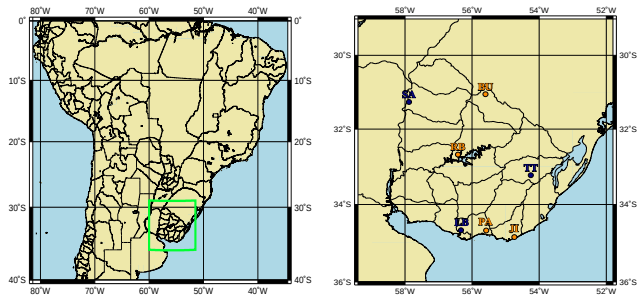

Figure 3: Geographical location and spatial distribution of the measurement stations. Blue: Kipp & Zonen CMP6 sensor. Orange: Li-Cor LI200SZ sensor. Station details are listed in Table 1.

reported in this work are based exclusively on GOES 13 images for the time period from may 2010 to december 2011. No correction factor was applied and we used directly the brightness counts, without conversion to radiances, as it was done in Justus et al. (1986). However, the model could be adjusted equally well using callibrated images with brightness converted to radiance.

3.2. Ground measurements

The solar irradiance ground data used in this work was collected during the years 2010 and 2011 from seven stations distributed over the territory of Uruguay. The geographical location of the measurement stations is indicated in Fig. 3 and further details are included in Table 1. Only the data collected in the time range May 2010 to December 2011 (i.e., when GOES 13 images were available) has been used for this work. Three of the stations (codes LB, TT and SA) are equipped with new Kipp & Zonen CMP6 pyranometers, located at sites of the National Institute for Agronomical Research (INIA). These equipments record global horizontal irradiance at one-minute intervals and are operated and maintained by our group. The other four stations (codes BU, PA, JI, RB), equipped with new Li-Cor LI200SZ photovoltaic sensors record average global horizontal solar irradiance at 10 minute intervals. These stations are owned and operated by the local public electric utility company (UTE).

Hourly irradiation data has been integrated from irradiance measurements for the same hourly intervals used to compute the mean brightness from the satellite images. Several consistency checks were run on the data and a small number of hours were discarded. For instance, the clarity index for hourly irradiation, k_T, (the ratio of hourly global horizontal irradiation

to the corresponding extraterrestrial value, see Iqbal (1983) for details) was used to discard about 1% of the data with $k_T > 0.8$. About 10% of the hours were discarded because no simultaneous satellite images were available. Daily totals were generated only for days with complete hourly records, *i.e.* no interpolation scheme for missing hours was used. No special corrections where applied to the Li-Cor sensors data to correct for spectral response, temperature dependence and cosine error (King and Myers, 1977, Myers, 2011).

4. Local implementation of the JPT model

In this Section we describe the local implementation of the JPT model for the target region shown in Fig. 3, which includes the whole territory of Uruguay and small parts of Brazil and Argentina. A first report on this implementation can be found in Alonso et al. (2011). Here, we summarize those results and provide updated estimates for the model coefficients and performance, due to an increased database.

Hourly average values of $\cos\theta_z$ and its powers, B_m and B_0, together with coincident ground measurements of hourly global irradiation were used to adjust the coefficients of Eq. (1), using a standard least-squares technique. The coefficients $\{a, b, c, d\}$ vary less than 5% when the model is adjusted using data from different sets. Thus we decided to use our own measurement network (codes LB, SA and TT sites) to train the model. These data is of controlled-quality, with the data acquisition and manipulation process under our control. These three sites provide adequate coverage of the target region, as shown in Fig. 3. We refer to this set as the *training set* (TRN). The rest of the stations listed in Table 1, provide independent measurements used to assess the model performance and are collectively referred as the *evaluation set* (EVA).

After primary filtering, the TRN set had 14858 hourly records and 845 daily records while the EVA set had 20472 hourly records and 964 daily records. The 14858 hourly data records from the TRN set were also filtered, discarding hours with $\cos\theta_z < 0.1$; these samples correspond to early morning or late afternoon hours which have insufficient illumination and may be affected by large cosine errors. A final training set of 13621 hours was obtained and used to adjust the coefficients. The coefficients obtained are shown in Table 2 and compared to those from the implementation in Justus et al. (1986). The general geographic characteristics of our target region (smooth grasslands with no snow cover, deserts or significant heights) are similar to those of the U.S. Great Plains. Hence, while being expected to differ from those reported by JPT, the coefficients of the clear-sky part of the model (a, b, c) should be of the same order of magnitude in both implementations. On the other hand, the d coefficient depends on the scaling of the brightness values, so in this case a comparison is meaningless.

Using Eq. (1) with the coefficients listed in the first row of Table 2, the hourly and daily global solar irradiation were estimated for each site in the evaluation group. The overall rRMS deviation was 18.6% on an hourly basis and 12.8% on a daily basis. These results considerably improve those previously obtained for the same region using Tarpley's coefficients developed for the U.S. (Frulla et al., 1988, 1990). Thus, a local adjustment of the coefficients is required for an acceptable performance of Tarpley's model. Fig. 4 shows the hourly scatter plot between ground data and the satellite-based estimates for the ensemble of testing sites. In this Figure, almost clear hours with $k_T > 0.65$ are indicated in blue and hours with $k_T \leq 0.65$ in green. This makes apparent that the JPT model underestimates irradiation for clear hours and mostly overestimates irradiation for cloudy hours. This bias is a known issue from this model (Justus et al., 1986). In order to reduce it while preserving the simplicity of the original model, we propose to introduce a brightness dependence in the model parameters and evaluate results by comparison with the independent testing data set. To distinguish this proposal from the original one by Tarpley, we call it Brightness-Dependent JPT or BD-JPT for short.

JPT coefficients	a	b	c	d (kJ/m^2)
This work	0.285	0.865	-0.392	-0.776
Justus et al. (1986)	0.415	0.717	-0.391	-1.630

Table 2: Coefficients for Eq. (1) obtained in this work from the training set, compared to the coefficientes reported by Justus et al. (1986).

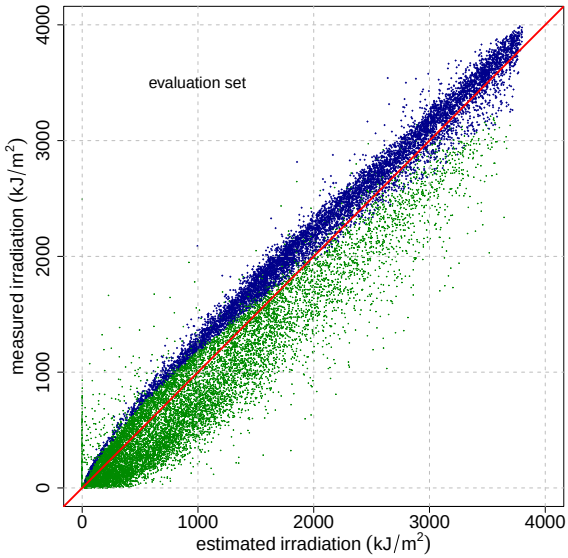

Figure 4: Scatter plot of ground data vs. satellite estimates from the JPT model (our implementation) for the EVA set on an hourly basis. Cloudy hours ($k_T \leq 0.65$) are shown in green and mostly clear hours ($k_T > 0.65$) are shown in blue. The measured value is used to calculate k_T. A diagonal red line has been drawn to indicate the perfect agreement case.

5. Brightness dependent (BD-JPT) model

The basic idea is to introduce brightness-dependence in the set of coefficients. The first decision to make is how many brightness subintervals should be considered. As mentioned before, visual inspection of Fig. 4 allows the identification of two kind of phenomena: (i) an accumulation of points just above the diagonal, which correspond to mostly clear-sky hours in which

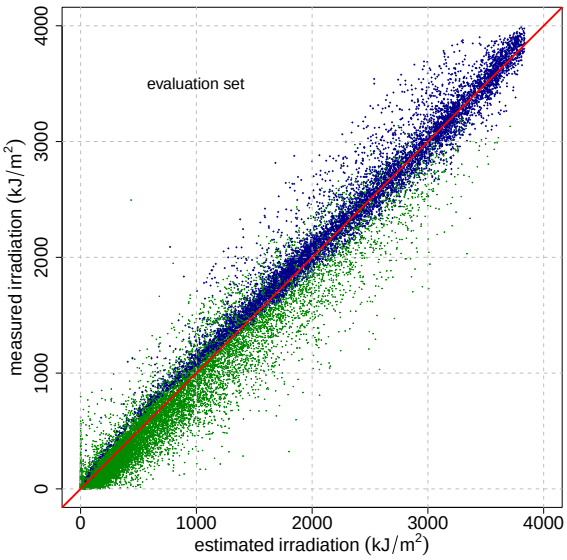

Figure 5: Scatter plot for hourly ground data vs. hourly estimates from the BD-JPT model for the four EVA sites. Green dots indicate cloudy hours, while blue dots correspond to mostly clear hours. The separation criteria is the same used in Fig. 4. The diagonal red line indicates the perfect agreement case.

irradiationis under-estimated and (ii) a pattern below the diagonal with larger spread, that corresponds mostly to cloudy hours in which solar irradiation is over-estimated. If these two sets of points (blue and green in Fig. 4) can be treated separately, the model performance should improve significantly. With the goal of keeping the model as simple as possible, we use only two brightness intervals which lead to two sets of parameters $\{a, b, c, d\}$ depending if the hour is classified as mostly clear or mostly cloudy.

For usability, the discrimination between both sets should be done on the basis of the satellite image information alone, i.e. on the B_m hourly values for a given position, since solar irradiation (or k_T) values are not available at arbitrary locations. Therefore, the second decision to be made is the choice of the threshold on normalized counts used to discriminate between mostly clear-sky hours and mostly cloudy hours. An optimum threshold value (in terms of the rRMS performance of the model) may be obtained from the data using minimization techniques. However, this optimum threshold would probably be location-dependent. For the sake of simplicity, we chose the mean brightness value, $\bar{B}_m$, from the normalized brightness data of the ensemble of training sites as a convenient threshold. This choice is ultimately supported by the good performance of the model. The median was also tested as a threshold, but it did not improve the results. In Fig. 1, the mean and median for the TRN set are indicated as vertical lines.

Thus, hours with $B_m \leq \bar{B}_m$ are considered as mostly clear hours, and a set $\{a_1, b_1, c_1, d_1\}$ is adjusted and used for irradiation estimation from Eq. (1) for these hours. On the other hand, hours with $B_m > \bar{B}_m$ are classified as mostly cloudy and a set $\{a_2, b_2, c_2, d_2\}$ is adjusted and used for them. For this implementation, the actual value obtained for $\bar{B}_m$ is 17.5 normalized counts.

BD-JPT coefficients	a	b	c	d (kJ/m^2)
mostly clear hours	0.363	0.918	-0.518	-2.521
mostly cloudy hours	-0.027	1.226	-0.502	-0.599

Table 3: Coefficients for Eq. (3), adjusted from the training set.

The BD-JPT model parametrization can be expressed as

$$I = \begin{cases} I_{sc}\,(r_0/r)^2 \cos\theta_z (a_1 + b_1 \cos\theta_z + \ldots \\ \qquad + c_1 \cos^2\theta_z) + d_1 \left(B_m^2 - B_0^2\right) & B_m \leq \bar{B}_m \\ I_{sc}\,(r_0/r)^2 \cos\theta_z (a_2 + b_2 \cos\theta_z + \ldots \\ \qquad + c_2 \cos^2\theta_z) + d_2 \left(B_m^2 - B_0^2\right) & B_m > \bar{B}_m. \end{cases} \quad (3)$$

The two sets of coefficients adjusted using the training set by standard least mean squares techniques are listed in Table 3. In the remainder of this section, we introduce the performance indicators and discuss the improvement in irradiation estimates that results from introducing brightness dependence in the model parameters.

5.1. *Performance indicators*

Statistical models are expected to perform significantly better when their estimates are compared with the training data than when the comparison is made against independent data. In the literature both kinds of comparisons are reported, and this may lead to confusion when comparing the performance of different models. For completeness, we report indicators with respect to both sets (training and evaluation). However, in order to assess the model performance we refer to the indicators from the independent (evaluation) data set. The comparison is done both on an hourly and a daily basis. We use the Root Mean Square deviation (RMS), Mean Bias Error (MBE) and R^2 indicators, which inform about the statistical behavior of the data, together with a Kolmogorov-Smirnov integral test (KSI) which provides information on the distance between the estimates distribution and the data distribution. The relative indicators, rRMS and rMBE, are expressed as a percentage of the mean value of the measured irradiation on the corresponding time basis.

5.2. *Komogorov - Smirnov test*

A two-sample Kolmogorov-Smirnov test is carried out to calculate two performance indicators (Espinar et al., 2009): KSI (Kolmogorov-Smirnov Integral) and OVER. Let us review their definitions and explain how they are computed. The first step is to compute estimators F for the Cumulative Distribution Functions (CDF) of the measured data and of its estimates. For a set of N values $S = \{X_1, X_2, \ldots X_N\}$. The empirical CDF is (Scott, 1992)

$$F(X) = \frac{1}{N} \#\{X_i \in S, X_i \leq X\} \quad (4)$$

where $\#\{\cdot\}$ stands for the cardinal (number of elements) in the set. The same procedure applied to the set of N estimates from a model, $\hat{S} = \{\hat{X}_1, \hat{X}_2, \ldots \hat{X}_N\}$, yields $\hat{F}(X)$. A distance between both CDFs, for each X, is defined as

$$D(X) = |F(X) - \hat{F}(X)|. \quad (5)$$

			JPT model performance						BD-JPT model performance					
Site	Hours	$< I >$ (MJ/m^2)	rRMS (%)	rMBE (%)	R^2	KSI (kJ/m^2)	rKSI (%)	rOVER (%)	rRMS (%)	rMBE (%)	R^2	KSI (kJ/m^2)	rKSI (%)	rOVER (%)
LB	4839	1.41	16.6	-0.5	0.953	54.0	61.4	5.8	12.1	-2.7	0.975	30.6	34.4	1.8
SA	4794	1.44	17.5	4.9	0.948	43.4	48.6	4.1	13.0	1.4	0.972	28.5	31.8	0.4
TT	5225	1.44	16.6	1.1	0.952	36.5	42.9	4.3	12.8	-2.3	0.971	23.2	26.8	0.2
TRN	**14858**		**16.9**	**1.8**	**0.951**	**44.4**	**50.8**	**4.7**	**12.6**	**-1.2**	**0.973**	**27.3**	**30.9**	**0.8**
BU	5356	1.46	19.1	3.7	0.941	65.8	77.8	22.1	14.5	3.5	0.967	54.3	63.6	9.3
JI	4958	1.44	17.1	-0.4	0.949	47.4	54.6	2.1	13.4	-0.7	0.968	22.8	25.8	0
PA	4743	1.35	21.4	2.7	0.924	58.1	65.9	16.8	15.8	1.7	0.958	37.2	41.6	3.0
RB	5415	1.43	17.0	-0.5	0.951	54.1	64.7	5.0	12.4	-0.1	0.974	23.3	27.7	0
EVA	**20472**		**18.6**	**1.4**	**0.941**	**56.5**	**66.0**	**11.5**	**14.0**	**1.1**	**0.967**	**34.5**	**39.9**	**3.1**

Table 4: Performance indicators for the JPT and the BD-JPT model estimates on an hourly basis for both the evaluation (EVA) and the training (TRN) sites. The averages, weighted with the number of hours in each station, are shown in boldface for the EVA and TRN sets. $< I >$ represents the hourly average of the measured data.

The null hypothesis that both sets (measurements and estimates) may belong to the same distribution is rejected with 99% confidence level if, for some X, $D(X)$ exceeds the critical value $V_c = 1.63/\sqrt{N}$ (Massey, 1951). The excess $O(X)$ by which $D(X)$ exceeds the threshold V_c is defined as

$$O(X) = \begin{cases} D(X) - V_c & \text{for} \quad D(X) > V_c, \\ 0 & \text{for} \quad D(X) \leq V_c. \end{cases} \tag{6}$$

Finally, the KSI and OVER indicators are computed as the areas KSI $= \int D(X)\,dX$ and OVER $= \int O(X)\,dX$, respectively. Relative indicators rKSI and rOVER are expressed as a percentage of the area below the threshold $V_c(X_{max} - X_{min})$, where X_{min} and X_{max} are the extreme values of $S \cup \hat{S}$. A positive OVER (or rOVER) indicates that the two-sample Kolmogorov-Smirnov test was not passed and the hypothesis that both data sets, measurements and estimates, belong to the same distribution is statistically rejected.

The application of this formalism to the case considered in this work is straightforward. The measured ground data is hourly global irradiation, I, at the evaluation sites and the estimated values are the models' estimates, $\hat{I}$, for the same hours at those sites. For each ensemble (training sites (TRN) and evaluation sites (EVA)), global indicators are computed as a weighted average of the indicators for each site, with weights proportional to the number of data points in each site.

5.3. Improvement due to Brightness Dependence

Hourly irradiation estimates were generated from both the JPT and the BD-JPT models for the seven ground stations. About 1% of the estimates which result in negative irradiation have been set to zero due to physical constrains.

Scatter plots for hourly irradiation estimates from the improved model vs. ground measurements from the EVA set are shown in Fig. 5. Visual inspection of this figure shows that the BD-JPT model achieves a significant reduction of the systematic deviations due to the underestimation of irradiation under clear-sky conditions and the overestimation under cloudy conditions, with respect to the hourly scatter plot of the JPT model, shown in Fig. 4.

The performance indicators for the hourly irradiation estimates from both the JPT and the BD-JPT models are summarized in Table 4. The BD-JPT model shows an important

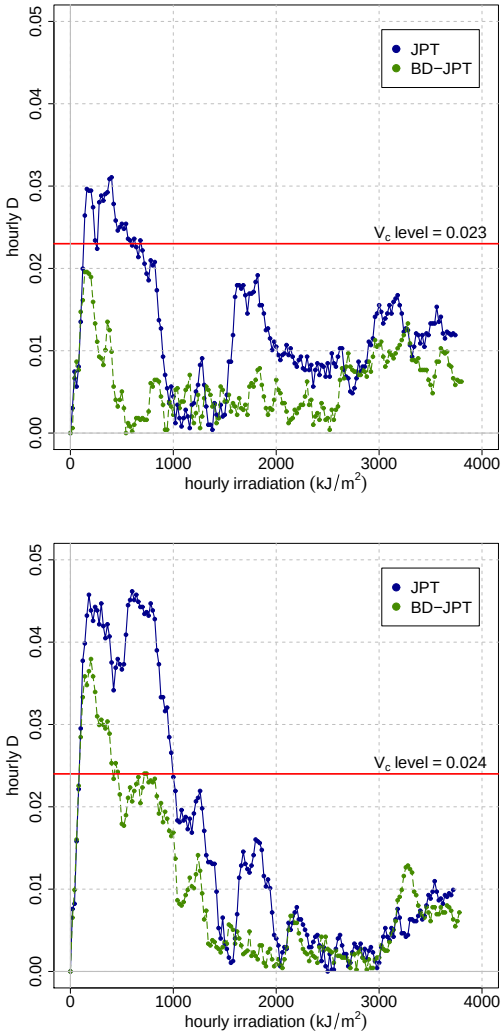

Figure 6: Distance between hourly distributions, D, defined in Eq. (5), in comparison with the V_c threshold level for the JI (upper panel) and PA (lower panel) sites of the EVA set. The blue symbols correspond to the JPT model and the green symbols to the BD-JPT model. See text for more details.

			JPT model performance						BD-JPT model performance					
Site	Days	$< H >$ (MJ/m^2)	rRMS (%)	rMBE (%)	R^2	KSI (MJ/m^2)	rKSI (%)	rOVER (%)	rRMS (%)	rMBE (%)	R^2	KSI (MJ/m^2)	rKSI (%)	rOVER (%)
LB	277	17.5	10.3	-0.1	0.965	0.63	22.6	0	5.3	-0.2	0.990	0.28	9.3	0
SA	265	17.9	10.6	0.3	0.957	0.63	21.3	0	6.1	1.4	0.986	0.37	11.9	0
TT	303	17.9	9.2	1.5	0.969	0.61	23.0	0	5.5	-0.2	0.988	0.32	11.0	0
TRN	**845**		**10.0**	**0.6**	**0.964**	**0.62**	**22.3**	**0**	**5.6**	**0.3**	**0.988**	**0.32**	**10.7**	**0**
BU	198	12.7	16.9	5.2	0.919	1.10	40.9	2.0	10.1	4.5	0.973	0.64	21.6	0
JI	287	17.9	9.7	-0.1	0.963	0.54	19.6	0	5.6	-0.9	0.988	0.32	10.6	0
PA	179	12.0	17.1	5.3	0.922	0.88	32.0	0	8.3	2.6	0.981	0.40	12.9	0
RB	300	17.4	10.6	0.2	0.967	0.57	21.0	0	5.8	0.1	0.988	0.27	9.0	0
EVA	**964**		**12.8**	**2.1**	**0.948**	**0.73**	**26.7**	**0.4**	**7.1**	**1.2**	**0.984**	**0.39**	**12.8**	**0**

Table 5: Performance indicators for the JPT and the BD-JPT models on a daily basis for both the evaluation (EVA) and the training (TRN) sites. $< H >$ represents the daily average of the measured data. The averages, weighted with the number of days in each station, are shown in boldface for the EVA and TRN sets.

decrease in rRMS and rKSI with respect to the JPT model. The comparison is meaningful because the estimates from both models are compared against the same independent (EVA) data set. For the JPT model, the evaluation results in an overall rRMS of approximately 19 % and rKSI of 66 %, while for the BD-JPT model these indicators are reduced to 14 % and 40 %, respectively. The rMBE index for both models yields comparable results showing small global bias in both cases.

Within the EVA set for the hourly comparison, two sets of stations can be distinguished by looking at their corresponding rOVER indicators in Table 4. On one side, the JI and RB sites exhibit low rOVER values; these rOVER values are also in reasonable agreement with those of the TRN sites. For these two stations, the BD-JPT model manages to achieve null rOVER; this was not the case for the original JPT model. On the other hand, the other two EVA stations (BU and PA) show the worst rOVER indicators under both models. For these stations, after on-site inspection, it was found that the sensors were shaded in the early morning hours during the summer months. Although some of these hours had been filtered out prior to models' validation, this may explain why these two stations show relatively poor agreement between estimates and data. In any case, the application of the BD-JPT model greatly reduced the rOVER values that resulted from the original JPT model for this pair of sites.

The improvement in the estimation of hourly irradiation obtained by the BD-JPT model is also illustrated in Fig. 6. In this figure, the EVA sites JI and PA are considered, to represent each of the pairs that was just singled out. For each of these stations, a panel shows the distance function D between the CDFs of hourly measurements and estimates, for both the JPT and BD-JPT models. For the case of JI (top panel), the small area above the V_c level for the JPT model corresponds to the non zero OVER indicator, as already outlined from Table 4. The application of BD-JPT leads to a D function that is completely below V_c, and implies that the null hypothesis that the set of measurements and the set of estimates are drawn from the same distribution cannot be rejected. For the PA station (bottom panel), the area above the V_c level for the JPT model is large: its rOVER is 16.8%.The BD-JPT model shows a major decrease in this area, reaching an rOVER of 3.0%.

The daily evaluation was carried out for 964 site-days. Daily irradiation estimates are generated by summation of the hourly

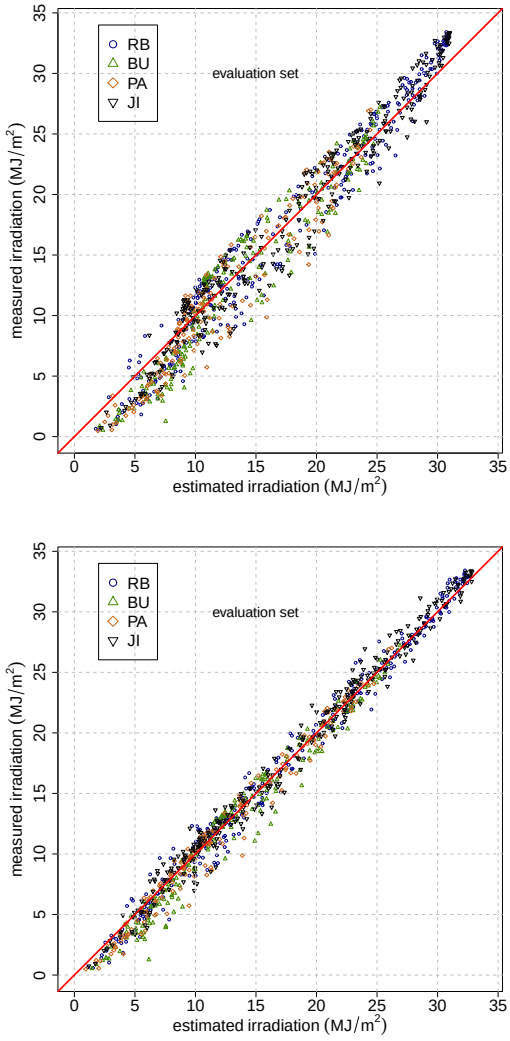

Figure 7: Scatter plots for daily ground data from the EVA sites vs. daily estimates for the JPT and the BD-JPT (lower) models. A diagonal red line has been drawn to compare with the ideal, perfect agreement situation.

estimates within each day. As expected, due to error cancellation in both models the daily indicators are much better than the hourly ones. The comparison indicators for a daily basis are summarized in Table 5. Specifically, the rRMS is reduced from 12.8% for the JPT model to 7.1% for the BD-JPT model. A

small over-estimating bias persists, but the BD-JPT model has a rMBE which is about half of the rMBE from the JPT model. The rKSI indicator for the BD-JPT models is less than half that of the JPT model, showing a significant reduction in the distance between both distributions (data and estimates). Except for the BU site, the daily rOVER parameter is zero in both models.

The improvement in daily agreement due to brightness-dependence is clearly illustrated in Fig. 7. Notice that the improvement in the daily indicators with respect to the hourly ones is much more dramatic in the case of BD-JPT. This is simply due to the fact that, in the scatter plots of hourly estimates (Figs. 4 and 5), the point cloud in the case of BD-JPT exhibits much more symmetry around its diagonal.

6. Conclusions

The model presented by Justus et al. (1986) (JPT model) for estimating hourly solar irradiation from GOES satellite images has been revisited and improved. A local implementation of the JPT model was developed for a territory that includes the plain grasslands of the subtropical eastern part of South America. Simultaneous irradiation measurements and GOES 13 images for the 2010-2011 period have been used. The model parameters were adjusted using controlled-quality solar irradiation data sets for three sites on our target territory (the training set). The model performance was evaluated against independent data sets for four sites (the EVA set) distributed over our target territory and an rRMS deviation of 12.8% was found. This local implementation of the JPT model yields acceptable results which represent a significant improvement with respect to previous evaluations of this model in the South American region. However, the JPT estimates are found to exhibit the characteristic biases for this model, consisting in a systematic underestimation of irradiation for clear-sky conditions and an overestimation for cloudy hours.

A brightness-dependent version of the model (the BD-JPT model) has been proposed as a way to reduce the systematic deviations observed in the JPT model, while preserving its simplicity. The formulation and implementation of the improved model has been explained in detail and two sets of parameters (for mostly clear and mostly cloudy sky conditions, respectively) have been adjusted using the training data set. A complete performance evaluation of both models has been conducted using independent measurements from the evaluation set on an hourly and on a daily basis. The performance indicators include the RMS deviation, the Mean Bias Error (MBE) and a Kolmogorov-Smirnov test that gives an indication of the distance between the cumulative distribution of the estimated values with respect to the one computed from the corresponding set of ground measurements.

Our results indicate that introducing a brightness-dependence in the model, as proposed in this work, significantly improves all the performance indicators, while preserving the simplicity of the original Tarpley formulation. Even though our proposal uses a simple two-interval brightness dependence using as a threshold the mean value of the brightness counts, the systematic bias present in the JPT model is significantly reduced. For irradiation estimates from the BD-JPT model, the rRMS is reduced to 7.1% on a daily basis and to 14.0% on an hourly basis. Deviations for two of the testing stations (BU, PA) are significantly worst than for the rest and this is traced to shading problems of these sensors in some early morning hours. So the performance of the BD-JPT model in this region is probably better than reported here.

Both methods (JPT and BD-JPT) are simple multiple regression models and the main difficulty in their implementation is the determination of the clear-sky brightness values from the images. We have tested the original iterative algorithm proposed by Tarpley (1979) for determining B_0, by replacing it with a standard filtering procedure based on RANSAC, a standard technique in robust estimation. The end results were not found to be significantly different in both cases, so Tarpley's algorithm, which is computationally more efficient has been used in the final formulation.

Even though previous works have assumed a some sort of universal validity (in space and over time) for the model parameters originally derived by Tarpley for the central U.S. area, we have shown that a local adjustment of the model parameters is required to obtain acceptable results in broadly separated areas, even if they are similar geographically. In fact, when the JPT model was applied to the central part of South America with the parameters adjusted for the U.S. Central area, rather poor results were obtained. Due to the statistical conception of these models, it should not be assumed that their parameters have a universal character. Even for regions with similar climate and geographical characteristics, such as the U.S. Great Plains and the target area of this work, some of the parameters vary appreciably. Probably, this may be the reason why Tarpley's model, in spite of its excellent balance between accuracy and simplicity, has not been used more extensively to estimate solar irradiation from satellite data.

With the brightness dependence proposed in this work, Tarpley's model can be an excellent tool for accurate solar irradiation estimation on an hourly or daily basis. In fact, when good-quality ground data are available to adjust the model, the accuracy of the daily irradiation estimates from the improved model may apporach the the typical uncertainty associated to radiometer measurements, but with a spatial resolution of a few kilometers.

Acknowledgements: We thank E. Cornalino and M. Draper for providing us with ground data from UTE, part of which was used as the evaluation set for this work. This work was supported by ANII under project FSE-2009-10-1, PEDECIBA and CSIC (Uruguay).

Alonso, R., Abal, G., Siri, R., Musé, P., 2011. Global solar irradiation assesment in Uruguay using Tarpley's model and GOES satellite images, in: Annals of the Solar World Congress (SWC 2011), Kassel, Germany.

Espinar, B., Ramirez, L., Drews, A., Beyer, H.G., Zarzalejo, L., Polo, J., Martin, L., 2009. Analysis of different comparison parameters applied to solar radiation data from satellite and German radiometric stations. Solar Energy 83, 118–125.

Espoz, C., Brizuela, A., 1983. Application of remote sensing and agrometeorological methods for crop assesment in the Pampa Húmeda. Technical Report ARG 81/002. FAO.

Fischler, M., Bolles, R., 1981. Random sample consensus: a paradigm for model fitting with applications to image analysis and automated cartography. Communications of the ACM 24.

Frulla, L., Gagliardini, A., Grossi Gallegos, H., Lopardo, R., 1988. Incident solar radiation on Argentina from the geostationary satellite GOES: comparison with ground measurements. Solar Energy 41, 61–69.

Frulla, L., Grossi Gallegos, H., Gagliardini, D., Atienza, G., 1990. Analysis of satellite-measured insolation in Brazil. Solar & wind technology 7, 501–509.

Hammer, A., 2003. Solar energy assessment using remote sensing technologies. Remote Sensing of Environment 86, 423–432.

Iqbal, M., 1983. An introduction to Solar Radiation. Academic Press.

Justus, C., Paris, M., Tarpley, J., 1986. Satellite-measured insolation in the United States, Mexico, and South America. Remote Sensing of Environment 20, 57–83.

King, D., Myers, D., 1977. Silicon photodiode pyranometers: operational characteristics, historical experiences and new calibration procedures, in: Proc. 26th IEEE Photovoltaic Specialists Conference, Anaheim, California.

Massey, F.J., 1951. The Kolmogorov-Smirnov test for goodness of fit. Journal of the American Statistical Association 46, 68–78.

Myers, D.R., 2011. Quantitative analysis of spectral impacts on Silicon photodiode radiometers. Technical Report NREL/CP-550-50936. National Renewable Energy Laboratory (NREL).

Noia, M., Ratto, C., Festa, R., 1993a. Solar irradiance estimation from geostationary satellite data: 1. statistical models. Solar Energy 51, 449–456.

Noia, M., Ratto, C., Festa, R., 1993b. Solar irradiance estimation from geostationary satellite data: 2. physical models. Solar Energy 51, 457–465.

Perez, R., 2002. A new operational model for satellite-derived irradiances: description and validation. Solar Energy 73, 307–317.

Perez, R., Seals, R., Zelenka, A., 1997. Comparing satellite remote sensing and ground network measurements for the production of site/time specific irradiance data. Solar Energy 60, 89 – 96.

Polo, J., Zarzalejo, L., Ramirez, L., 2008. Solar radiation derived from satellite images, in: Badescu, B. (Ed.), Modelling Solar Radiation at the earth's surface: Recent Advances. Springer. chapter 18.

Righini, R., Barrera, D., 2008. Empleo del modelo de Tarpley para la estimación de la radiación solar global mediante imágenes satelitales GOES en Argentina. Avances en Energías Renovables y Medio Ambiente 12, 9–15.

Rigollier, C., 2004. The method heliosat-2 for deriving shortwave solar radiation from satellite images. Solar Energy 77, 159–169.

Scott, D.W., 1992. Multivariate Density Estimation: theory, practice, and visualization. Wiley and Sons.

Stoffel, T., Renné, D., Myers, D., Wilcox, S., Sengupta, M., George, R., Turchi, C., 2010. Best Practices Handbook for the Collection and Use of Solar Resource Data. Technical Report NREL/TP-550-47465. National Renewable Energy Laboratory (NREL).

Tarpley, J., 1979. Estimating incident solar radiation at the surface from geostationary satellite data. Journal of Applied Meteorology 18, 1172.

Zarzalejo, L.F., Polo, J., Martín, L., Ramírez, L., Espinar, B., 2009. A new statistical approach for deriving global solar radiation from satellite images. Solar Energy 83, 480–484.